Available online at www.sciencedirect.com
SCIENCE DIRECT
Lithos 90 (2006) 1–18
LITHOS
www.elsevier.com/locate/lithos

Baddeleyite-apatite-spinel-phlogopite (BASP) rock in Achankovil Shear Zone, South India, as a probable cumulate from melts of carbonatite affinity

V.J. Rajesh [a,*], S. Arai [b]

[a] Department of Earth and Environmental Sciences, Basic Science Research Institute, Chonbuk National University, Chonju 561-756, South Korea
[b] Department of Earth Sciences, Graduate School of Natural Science and Technology, Kanazawa University, Kakuma, Kanazawa 920-1192, Japan

Received 26 August 2005; accepted 9 January 2006
Available online 13 March 2006

Abstract

We report here the petrography, mineralogy and in-situ trace-element mineral geochemistry of a rare and hitherto unidentified baddeleyite-apatite-spinel-phlogopite (BASP) rock in Late Neoproterozoic Achankovil Shear Zone (ACSZ) in South India. The rock unit occurs as isolated outcrops and demarcates the western boundary of an ultramafic complex in ACSZ. The modal mineralogy of the BASP rock is baddeleyite < apatite < spinel < phlogopite. Baddeleyite is found as inclusions within spinel and phlogopite. The spinel is highly aluminous with copious inclusions of high-T melts, pure CO_2-fluids, magnesite and graphite. Apatite is the major carrier of halogens such as F and Cl, LREEs, U and Th, and phlogopite is the robust reservoir of Ba and Rb. The concentrations of REE in apatite are quite variable (ΣREE ~ 7646–13485 ppm), but the chondrite normalized patterns show a uniform negative sloped REE patterns with significant negative Eu anomaly, which is indicative of the crystallization of apatite in a reduced environment. The mineral assemblage of apatite–phlogopite–baddeleyite is typical of carbonatites from various carbonatite complexes. Moreover, the LREE enrichment and negative Eu anomaly of apatite, low Ti and Fe, and high Al, Mg, Ba and Rb of phlogopite, as well as actinide enrichment of baddeleyite relative to REEs, are characteristic signatures of carbonatites from various tectonic settings. Therefore, we argue that the BASP rock is probably formed by crystal precipitation from melts having carbonatite affinities derived from the upper mantle and emplaced into the lower crustal level during the extensional collapse of the orogen following the collisional assembly of the Gondwana supercontinent. The deep-rooted ACSZ acted as the pathway for the infiltrating melts.

Keywords: Baddeleyite; Apatite; Aluminous spinel; Phlogopite; Carbonatite; Achankovil Shear Zone

1. Introduction

Shear zones in high-grade metamorphic terrains often exert significant control over the exhumation history of continental deep crust, emplacement tectonics of igneous intrusives, and transfer of unusual fluids/melts from various depths (e.g. McCaig, 1997; Cartwright et al., 1999). They also serve as loci for a variety of mineralization (Mikuchi and Ridley, 1993). Among a suite of magmatic plutons associated with various shear zones in high-grade terrains, silica-undersaturated rocks are of particular importance since they offer windows into processes from the deep crust through crust–mantle

* Corresponding author. Tel.: +82 63 270 3397.
E-mail address: rajeshvj@chonbuk.ac.kr (V.J. Rajesh).

0024-4937/$ - see front matter © 2006 Elsevier B.V. All rights reserved.
doi:10.1016/j.lithos.2006.01.004

interface to the upper mantle. The continental fragments derived from East Gondwanaland consist of a collage of high-grade metamorphic terrains, which are dissected by major transcrustal shear zones. The Late Neoproterozoic Achankovil Shear Zone (ACSZ) in southern India is an example, which is characterized by highly deformed granulite facies supra-crustal rocks and orthogneisses that are variously intruded by felsic plutons, mafic dykes and ultramafic bodies. In this paper, we report the results of petrography, and major- and trace-element mineral chemistry on an undeformed and unmetamorphosed, rare and unusual, baddeleyite-apatite-spinel-phlogopite (BASP) rock within the ultramafic complex of Achankovil Shear Zone (ACSZ), South India. This will contribute to the unraveling of a peculiar deep-seated process related to the behaviors of melts of carbonatite affinities that has never been documented.

2. Geological setting and outline of the ultramafic complex

The study area, around Perunthol village is located in the Kollam district of Kerala and lies within the Late Neoproterozoic Achankovil Shear Zone (ACSZ) in Southern Granulite Terrain (SGT) (Fig. 1a). ACSZ is widely recognized in the literature as a major transcrustal shear zone (e.g. Drury and Holt, 1980; Rajaram et al., 2003) and has received broad attention in Gondwana correlation studies (e.g. Windley et al., 1994; Kröner and Brown, 2005). The ACSZ is a dominant NW–SE trending strike-slip shear zone that appears as a major lineament in aeromagnetic and satellite images, and separates a vast supracrustal sequence of Trivandrum Block (TB) that lies in the south of the shear zone from predominantly granulite facies rocks of Madurai Block (MB) in North (Drury et al., 1984; Harris et al., 1994). All these blocks were subjected to polyphase ductile deformation, granulite facies metamorphism and crustal rejuvenations during the Pan-African Orogeny (Brandon and Meen, 1995; Braun et al., 1998; Braun and Kriegsman, 2003; Santosh et al., 2003, 2005; Cenki et al., 2004). The dominant rocks within ACSZ are represented by intensely deformed and migmatized garnet-biotite gneiss, khondalite, cordierite and quartzofeldspathic gneiss, charnockites and calc-silicates (Santosh, 1987, 1996 and references therein). They were intruded by partly to totally undeformed felsic rocks, such as granite, pegmatite, monzonites, quartz diorite and basic to ultramafic rocks like gabbro, dolerite and rare ultramafic rocks (Rajesh et al., 1996; Rajesh, 2004a,b; Rajesh et al., 2004a; Santosh et al., 2005). The metamorphic grade throughout the shear zone ranges from ultra-high temperature to high-temperature part in granulite facies (e.g. Nandakumar and Harley, 2000). The predominant granulite facies metamorphisms were dated back to be of the Pan-African period (e.g. Bartlett et al., 1998; Cenki et al., 2004). Most of the felsic intrusives were also dated to be Late Pan-African by various methods (Rajesh, 2004a; Santosh et al., 2005).

A comprehensive portrayal of the geological aspects of the rare rock units constituting the ultramafic complex in ACSZ is given in Rajesh et al. (2004a,b), and is briefly summarized here. The rarity of outcrops and thick soil cover hindered the direct observation of the relation of the BASP rock with the other rock units of ultramafic complex and the surrounding high-grade metamorphic rocks. This unique ultramafic complex is composed of spinel dunite (olivine + spinel + phlogopite + dolomite ± ilmenite ± rutile + serpentine), phlogopite dunite (olivine + phlogopite + dolomite ± ilmenite ± rutile ± brucite ± baddeleyite + serpentine), glimmerite (phlogopite ± ilmenite ± rutile), graphite-spinel glimmerite (phlogopite + spinel + graphite ± baddeleyite) and phlogopite-graphite spinellite (spinel + graphite ± zirconolite ± phlogopite) from SE to NW (Fig. 1b). Based on bulk rock and mineral chemistry, stable C and O isotopes, and fluid inclusion studies Rajesh (2004b) interpreted that the ultramafic complex was formed by the differentiation and crystallization of highly potassic and volatile (H_2O and CO_2) rich melts of probable upper mantle origin. Subsequently these melts were emplaced into lower crustal levels through the deep-rooted shear zone (which acted as the pathway for the infiltrating fluids) after the dominant Pan-African tectonothermal events. The complex was dated to be Early Ordovician by U–Pb electron microprobe ages of zirconolite and K–Ar ages of phlogopite (Rajesh, 2004b; Rajesh et al., 2004a,b, in press).

The investigated rocks are found in the northwestern limit of the ultramafic complex and occur as an isolated exposure in the streambed in close proximity to the phlogopite–graphite spinellite. The rock is medium-grained with interlocking texture and is melanocratic. Megascopically visible constituent minerals are randomly oriented with no perceptible deformations in the rock, which is in sharp contrast to the highly deformed nature of the surrounding high-grade metamorphic rocks. The rock appears to be very fresh meagascopically even though phlogopite forms the predominant mineral (Fig. 2). The spinel is almost colorless to pale violet, phlogopite is glittering pale black to dark brown and apatite is light greenish in color in hand specimen. At places, relatively coarse grains of apatite (~0.5 cm in

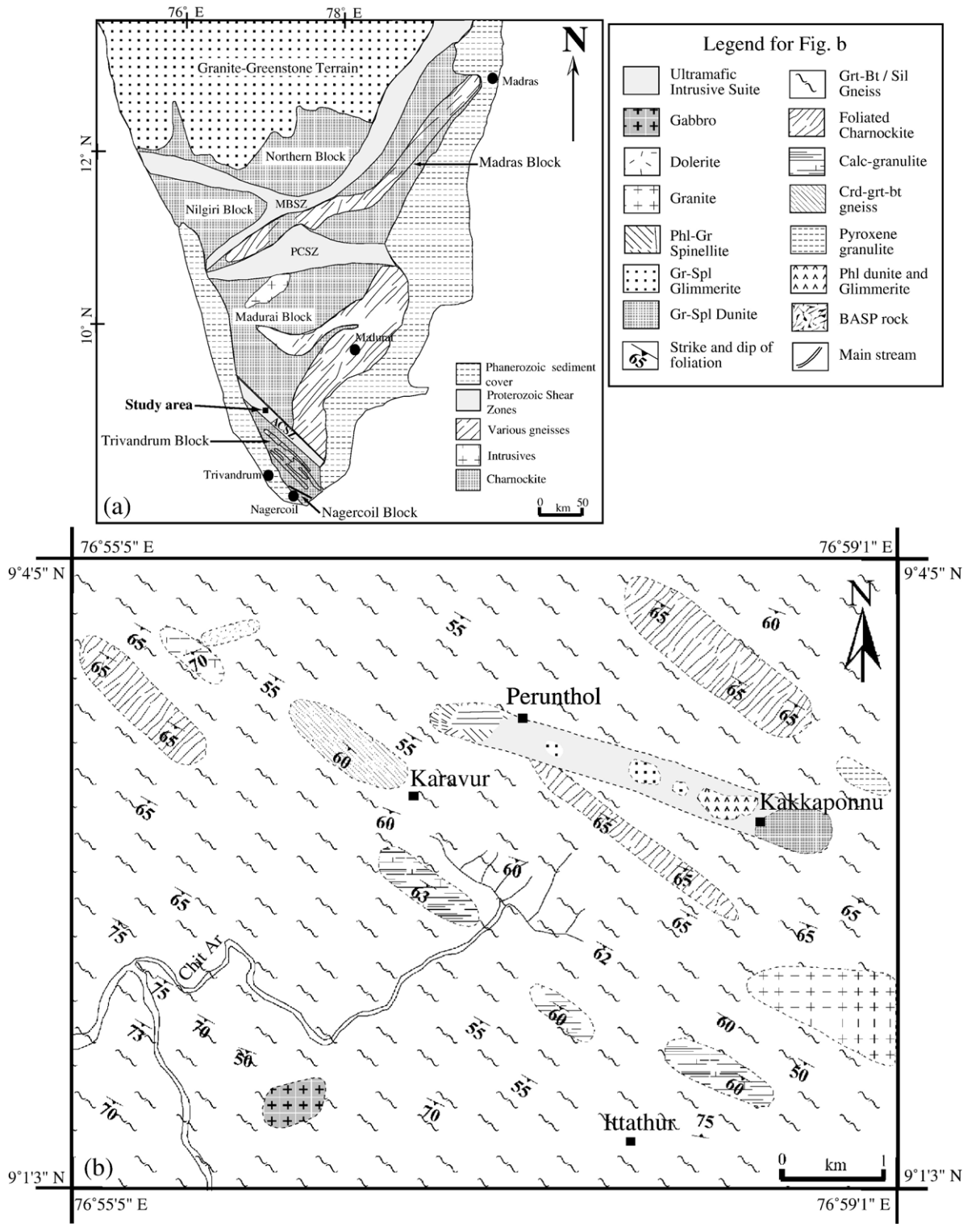

Fig. 1. (a) Tectonic setting of southern granulite terrain (SGT) showing the major granulite blocks, Late Neoproterozoic transcrustal shear zones and location of the study area. MBSZ: Moyar Bhavani Shear Zone, PCSZ: Palghat Cauvery Shear Zone and ACSZ: Achankovil Shear Zone. (b) Simplified geological map of the studied area showing extent of the ultramafic intrusive and other lithologies (modified after Rajesh et al., 2004a).

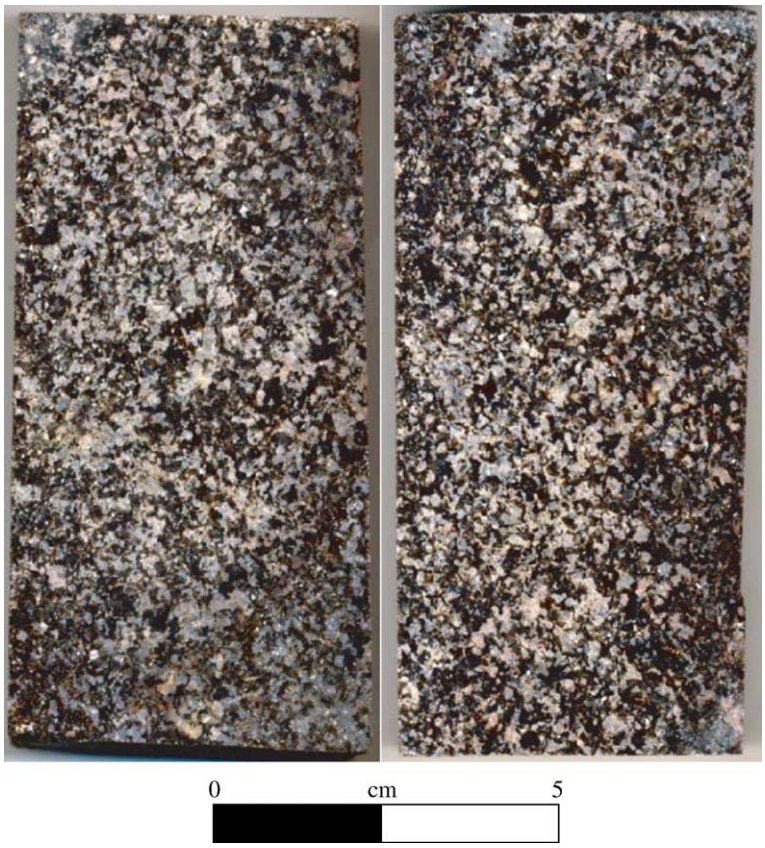

Fig. 2. Polished slabs of BASP rock.

length; subhedral to euhedral) found associated with phlogopite and spinel are noticed. The mineral species of the rock itself reveal its silica-undersaturated nature. Combined with the absence of any deformational features in contrast to the surrounding high-grade metamorphic rocks we foresee that the BASP rock also forms the part of the ultramafic complex, and delineates its western limit. Moreover, the mode of occurrence of this rock as isolated outcrop is largely not in agreement with a metasedimentary origin.

3. Petrography

Spinel (~40 vol.%), phlogopite (~40–45 vol.%) and apatite (~15 vol.%) are the foremost constituents of the rock. A characteristic feature of this rock is the interlocking texture defined by apatite, spinel and phlogopite (Fig. 3a and e). No textural features indicative of mineral replacement were observed. All the minerals are very fresh and even phlogopite shows no signs of alteration at all. All of the three minerals, apatite, spinel and phlogopite, have sharp contacts with each other (Fig. 3a and e). The spinel and apatite show high relief. The spinel is mostly anhedral, and apatite in general is anhedral to subhedral, but shows well developed hexagonal symmetry at places. Phlogopite is mostly tabular to prismatic with its characteristic cleavage. The spinel is colorless to white, and apatite is pale grayish in color in thin section. Phlogopite is pleochroic with various shades of yellowish brown to pale brown. The coarser grains of apatite and spinel are fractured (Fig. 3a, c), but phlogopite is least fractured. The spinel present in this rock has abundant CO_2-rich fluid (Fig. 3b,c) and melt inclusions (Fig. 3d). At places we found coexistence of CO_2–graphite, CO_2–magnesite, and magnesite–graphite inclusions within the spinel (Fig. 3c). In general, apatite and phlogopite do not have any inclusions, but we found only one subhedral grain of apatite hosting aligned needle-like inclusions (Fig. 3e). The composition of the inclusions has not been determined, as they are not exposed to the surface. At several places, apatite is found as inclusions within the fracture planes of spinel (Fig. 3a). These apatites are highly fresh and unfractured. Baddeleyite is very rare and small in size: minute grains of baddeleyite (<1 vol.%) are observed as inclusions within spinel

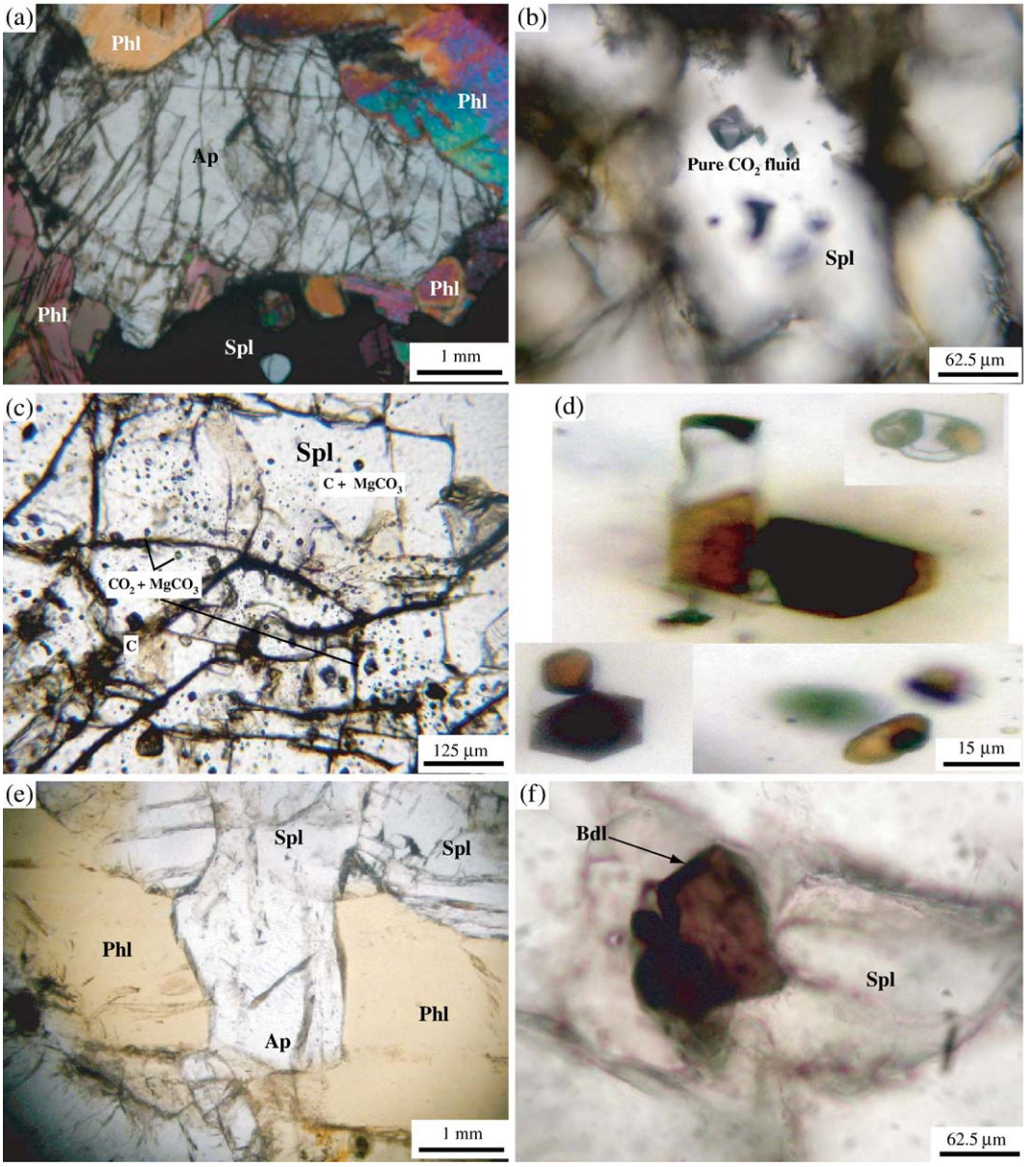

Fig. 3. Photomicrographs of the BASP rock. Ap, apatite; Phl, phlogopite; Spl, spinel; Bdl, baddeleyite; and C, graphite. All are by plane-polarized light except for (a). (a) Coarser apatite grain in sharp contact with phlogopite and spinel (crossed-polarized light). (b) Isolated primary pure CO_2 inclusion within the spinel. (c) Abundant CO_2, graphite and magnesite inclusions within the spinel. Please note the coexistence of graphite–magnesite and CO_2–magnesite. (d) High-T biphase melt inclusions observed within the spinel. (e) Aligned needle like inclusions noticed in a subhedral apatite grain that is in sharp contact with spinel and phlogopite. (f) Baddeleyite found as inclusion within the spinel grain.

(Fig. 3f) and phlogopite at places, suggestive of its earlier crystallization as described previously by Rajesh et al. (in press) on the other rock types of this ultramafic complex. The baddeleyite grains are anhedral, with translucent dark brown color. The characteristic polysynthetic twinning of baddeleyite (Heaman and Le Cheminant, 1993) is weakly noticeable.

4. Methods of investigation of mineral chemistry

4.1. Major elements

The mineral chemical compositions were determined with a JEOL JXA-8800R Superprobe (WDS) situated at Kanazawa University, Japan. The analyses

were performed with the following analytical conditions, an accelerating voltage of 15 kV, a probe current of 12 nA and probe diameter of 3 μm. The analyses were refined using the ZAF online correction program.

4.2. Trace and rare earth elements

Apatite, phlogopite and spinel were analyzed for trace and rare earth elements in-situ by a Laser Ablation (193 nM ArF excimer: MicroLas GeoLas Q-plus)-Inductively Coupled Plasma Mass Spectrometry (ICP-MS: Agilent 7500S) installed at the Incubation Business Laboratory Center of Kanazawa University. Only two grains of baddeleyite were detected but they were too small for a LA-ICP-MS analysis. Thus, we did not try to analyze baddeleyite grains. Moreover, the EPMA analyses on baddeleyite grains of other rock units revealed the absence of significant amount of trace elements apart from actinides (Rajesh et al., 2004b, in press). Each analysis of apatite, phlogopite and spinel was executed by ablating 20 μm, 100 μm and 100 μm diameter spots, respectively, at 5 Hz with an energy density of 8 J/cm^2 per pulse. The NIST SRM 610 and 612 glasses were used as the primary calibration standards. The element concentrations of NIST SRM 610 and 612 glasses for calibrations are the values compiled by Pearce et al. (1997). The primary calibration standards were analyzed routinely at the beginning and end of each batch of 3–4 samples. A linear correction drift was applied between each calibration. The machine conditions and procedure for analyses were best illustrated by Ishida et al. (2004). Also the analytical details and the quality of data were described in Morishita et al. (2005). The data reductions were aided by using Ca as internal standard for apatite and Si for phlogopite based on the CaO and SiO_2 contents (in wt.%) determined by EPMA analyses, following a protocol essentially identical to that outlined by Longerich et al. (1996). Since there are no sharp compositional variations among the core and rim analyses of apatite and phlogopite grains by microprobe analyses, we applied CaO wt.% and SiO_2 wt.% as the internal standards for apatite and phlogopite, respectively.

5. Results

5.1. Baddeleyite

Due to the rarity and small grain size, we could analyze only three points on baddeleyite grains. The analyzed grains consist of ZrO_2 (~96.52–97.04 wt.%) and HfO_2 (~2.13–2.43 wt.%), with minor amounts of UO_2 (~0.10–0.25 wt.%) and TiO_2 (~0.23–0.40 wt.%). Representative analyses of baddeleyite are listed in Table 1.

5.2. Apatite

The concentrations of major, trace and rare earth elements of selected apatite grains are given in Table 2. Their major-element compositions including the halogens indicate that the apatite falls in the middle field of solid solutions between the end members hydroxyl-apatite, fluor-apatite and chlor-apatite (Treloar and Colley, 1996; Fig. 4). CaO and P_2O_5 do not display any systematic intra-grain variations. However, F (1.73–2.29 wt.%) shows slightly higher values towards the core and the reverse is observed for Cl (2.89–3.29 wt.%). Minor amounts of SrO (0.25–0.56 wt.%) and SiO_2 (0.39–0.96 wt.%) are also noticed in apatite. The total REE contents of apatite vary from 7646 to 13485 ppm. This variation is not systematic, but can be observed among grains and even inside the single grains. According to Seifert et al. (2000) and Belousova et al. (2001), these variations are primarily

Table 1
Representative baddeleyite compositions

Anal. no.	sgl1-1	sgl1-2	sgl2-1
TiO_2	0.40	0.44	0.23
FeO	0.00	0.05	0.03
CaO	0.00	0.02	0.05
ZrO_2	96.52	96.69	97.04
HfO_2	2.43	2.13	2.28
UO_2	0.25	0.10	0.19
Y_2O_3	0.00	0.03	0.00
La_2O_3	0.00	0.00	0.00
Ce_2O_3	0.00	0.10	0.00
Nd_2O_3	0.00	0.00	0.00
Sm_2O_3	0.13	0.00	0.00
Gd_2O_3	0.17	0.25	0.25
Total	99.90	99.81	100.07
Formulae based on 2 atoms of oxygen			
Ti	0.006	0.007	0.004
Fe	0.000	0.001	0.000
Ca	0.000	0.000	0.001
Zr	0.977	0.977	0.980
Hf	0.014	0.013	0.013
U	0.001	0.000	0.001
Y	0.000	0.000	0.000
La	0.000	0.000	0.000
Ce	0.000	0.001	0.000
Nd	0.000	0.000	0.000
Sm	0.001	0.000	0.000
Gd	0.001	0.002	0.002
Σ cations	1.000	1.001	1.001

Table 2
Representative major, trace and REE analyses of apatite

Anal. no.	sgl1-c1a	sgl1-c4a	sgl1-c5a	sgl3c3a4	sgl1-c5ar	sgl2c3a2	sgl2c3a3	sgl2c3a1	sgl2c3a4	sgl3c3a2	sgl3c3a1	sgl3c3a3
	Core	Rim	Core	Rim	Rim	Core	Core	Rim	Rim	Core	Rim	Core
SiO_2	0.70	0.77	0.77	0.45	0.58	0.45	0.86	0.84	0.94	0.52	0.73	0.94
CaO	53.73	54.52	54.19	54.28	54.63	54.74	54.56	54.08	53.98	54.81	54.33	54.03
SrO	0.56	0.49	0.43	0.52	0.36	0.38	0.25	0.32	0.34	0.31	0.28	0.29
P_2O_5	39.24	41.31	40.41	40.58	40.64	41.77	41.15	40.04	40.04	40.74	40.10	39.87
F	1.77	1.91	2.07	1.73	1.90	1.95	2.02	1.85	1.92	2.29	2.15	1.77
less O	0.75	0.80	0.87	0.73	0.80	0.82	0.85	0.78	0.81	0.96	0.90	0.75
Cl	3.10	3.12	3.05	3.29	3.15	3.21	2.89	3.10	3.21	2.94	2.98	2.92
less O	0.70	0.71	0.69	0.74	0.71	0.72	0.65	0.70	0.72	0.66	0.67	0.66
Total	97.65	100.61	99.36	99.38	99.75	100.96	100.23	98.75	98.90	99.99	99.00	98.41
B	80	107	106	62	81	99	101	60	54	81	47	75
Mg	2783	642	1216	501	658	1177	1174	575	485	659	468	583
Ti	15	27	11	24	23	12	bdl	19	21	29	23	24
V	10	5	11	3	5	10	10	3	3	4	2	4
Mn	346	279	406	244	302	415	427	309	244	328	238	279
Fe	827	440	674	337	388	663	592	383	296	425	278	358
Ga	bdl	12	1	3	3	1	1	2	2	2	2	3
Ge	15	34	17	24	32	16	15	29	21	23	18	26
Sr	3463	2667	3993	2675	2646	3866	3951	2750	2711	2623	2600	2556
Y	1707	2969	1986	2423	2998	1895	1919	2798	1981	2086	1833	2329
Zr	14	12	14	5	12	12	12	13	6	5	4	6
Nb	bdl	0	0	0	0	0	bdl	0	0	0	0	0
Ba	24	224	18	52	26	17	15	25	18	20	23	30
La	1372	1515	1467	2106	1458	2040	2537	1855	2493	1752	2380	1601
Ce	3084	3377	3230	4701	3216	4507	5614	4160	5503	3789	5154	3551
Pr	360	394	375	526	372	511	637	459	624	426	592	395
Nd	1455	1630	1569	2081	1552	2013	2532	1864	2483	1722	2432	1584
Sm	324	356	338	428	334	412	520	373	516	355	491	316
Eu	50	54	51	44	52	43	54	39	53	35	49	32
Gd	303	348	327	408	322	393	512	361	490	334	473	310
Tb	49	56	52	64	52	61	78	55	77	52	74	47
Dy	290	331	315	368	313	363	468	332	460	303	439	278
Ho	60	69	65	78	65	75	96	67	95	63	90	57
Er	153	176	168	194	169	185	240	168	243	158	226	144
Tm	20	29	22	24	29	21	21	27	19	20	17	23
Yb	113	127	121	127	120	123	158	110	158	101	149	94
Lu	13	15	14	14	14	14	19	13	18	12	17	11
W	29	26	25	14	23	35	34	16	8	11	9	15
Pb	48	68	65	48	72	58	60	60	41	54	35	49
Bi	1	1	1	1	1	1	1	1	0	1	0	1
Th	359	842	420	630	812	357	347	759	388	413	307	480
U	333	665	349	428	659	305	301	544	277	323	191	380
$(La/Yb)_N$	8.7	8.5	8.7	11.9	8.7	11.9	11.5	12.1	11.3	12.5	11.5	12.3
Eu_N/Eu^*	0.5	0.5	0.5	0.3	0.5	0.3	0.3	0.3	0.3	0.3	0.3	0.3

due to the change in parental melt composition during fractionation. Nevertheless, the systematic variation from core to rim is not observed. The apatites are LREE-enriched relative to HREEs with the chondrite normalized $(La/Yb)_N$ ratio ranges from 8.5 to 12.5. This results in a steep negative REE patterns with significant negative Eu anomaly in the chondrite normalized diagram (Fig. 5). The Eu/Eu* (Eu anomaly) ratios are between 0.31 and 0.49. The higher $(La/Yb)_N$ also indicates strong LREE fractionation into apatite. The apatite is also rich in U (191–665 ppm) and Th (307–842 ppm).

5.3. Spinel

The spinel exhibits very limited compositional variations (Tables 3a and b). Small variations in Al_2O_3 and FeO contents are observed among the rim and core

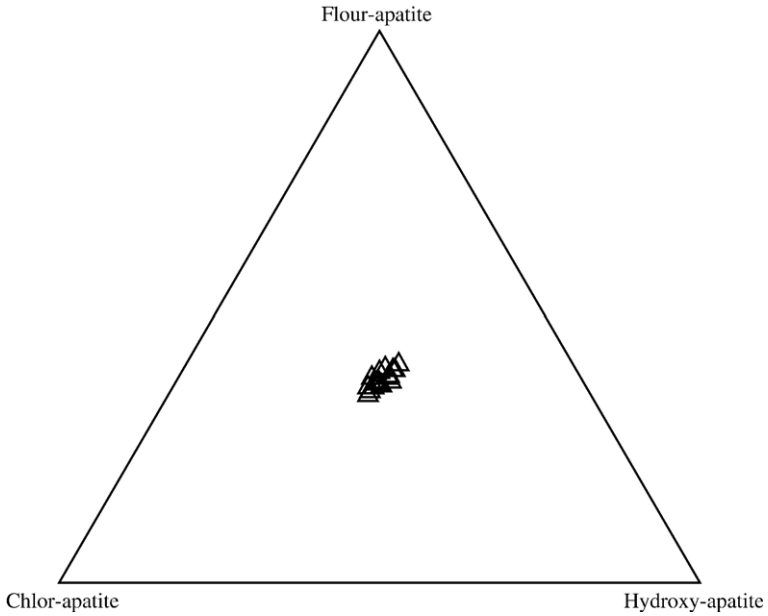

Fig. 4. Apatite composition in terms of F (fluor), Cl (chlor) and OH (hydroxy) contents.

analyses, although not systematic. The spinel is highly aluminous with high contents of Al_2O_3 (68.57–70.05 wt.%) and MgO (23.04–23.89 wt.%). The notable features of these spinel are low TiO_2 (0.00–0.03 wt.%) and Cr_2O_3 (0.02–0.09 wt.%) contents. Minor amounts of MnO (0.10–0.19 wt.%) is also noticeable. The Mg# (100*Mg/{Mg+Fe^{2+}} atomic ratio) varies from 85 to 86. The EPMA and semi-quantitative LA-ICP-MS analyses on spinel (Tables 3a and b) reveal its low trace element abundances: Ti (7.1 ppm), V (44 ppm), Ni (14.7 ppm), Co (7.1 ppm) and Zn (304.5 ppm). Zr (0.2 ppm), Hf (0.2 ppm), Th (0.1 ppm) and U (0.1 ppm) are also detected in spinel. The ΣREE (~1.8 ppm) abundances are very low with relative enrichment of HREE over LREE.

5.4. Phlogopite

All analyzed grains of phlogopite show some core-to-rim chemical variations that are not systematic. Al_2O_3 and K_2O with the values range from 17.88 to 19.00 and 10.13 to 10.57 wt.%, respectively. It shows characteristically low contents of Na_2O (0.10–0.19 wt.%). The phlogopite is poor in TiO_2 (0.85–1.16 wt.%) and Cr_2O_3 (0.00–0.04 wt.%). The total FeO ranges from 1.85 to 2.37 wt.%. The phlogopite thus shows very high Mg# (100*Mg/{Mg+Fe} atomic ratio) around 95–96. The K/(K+Na) ratio of phlogopite is very high, 0.97–0.99, being similar to deep-seated mantle phlogopites (Arai, 1986). All the phlogopites analyzed have appreciably higher contents of eastonite component, with 5.4 to 5.5 Si atoms based on O=22 (anhydrous basis) (Table 4a). The qualitative chemical analysis disclosed the extremely low amounts (most cases below detection limits) of halogen contents (F and Cl) in the phlogopite. LA-ICP-MS analysis revealed the absence of REEs in phlogopite. Instead, they are enriched in trace elements such as Ba (1601–1874 ppm), Rb (638–696 ppm), Sr (48–105 ppm), Nb (26–31 ppm) and Zr (9–27 ppm). The representative chemical compositions of phlogopite by EPMA and LA-ICP-MS are presented in Tables 4a and b. The analyses show that phlogopite is superior sink for some trace elements such as Ba, Rb and K in the upper mantle.

6. Discussion

6.1. Mineral paragenesis and chemistry

Rocks with baddeleyite–apatite–phlogopite mineral assemblages are typical of ore bodies that have been ultimately derived from alkaline-magmas of carbonatite-affinities. The extreme cases are the carbonatite complexes of Kovdor (Russia), Palabora or Phalaborwa (South Africa) and Jacupiranga (Brazil). The occurrence of aluminous spinel in association with baddeleyite–apatite–phlogopite made the rocks of present study highly unusual, as aluminous spinel cannot be formed straightforwardly from an ultramafic magma (such as lamproitic or kimberlitic; e.g. Wagner and Velde, 1987).

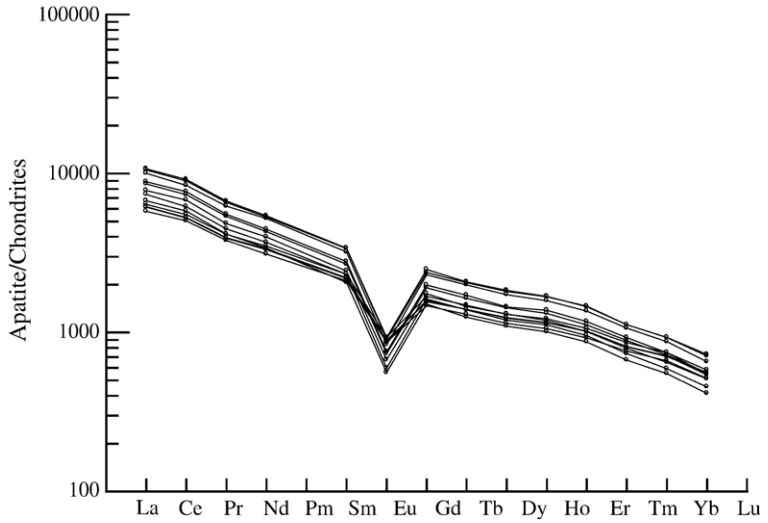

Fig. 5. Chondrite-normalized (Sun and McDonough, 1989) REE patterns for apatite.

Most of the spinels settled from ultramafic magma are Cr-rich or chromite (Dick and Bullen, 1984; Arai, 1992, 1994a,b; Schulze, 2001) owing to the very high partition coefficient of Cr into the spinel (Irving, 1978; Jaques and Foley, 1985; Sack and Ghiorso, 1991). Even so, there have been few reports on the occurrence of aluminous spinel in ultramafic rocks like lamproites. Aluminous spinel as a matrix and inclusion minerals within lamproites were described from Western Australia (Jaques and Foley, 1985; Wagner and Velde, 1987), ultrapotassic lavas of Leucite Hills (Keuhner et al., 1981) and Spain (Venturelli et al., 1984). In addition, aluminous spinel was found as needle-like inclusion in olivine in spinel peridotite xenoliths from Bismark

Table 3a
Representative analyses of spinel

Anal. no.	sgl1-c1a	sgl1-c4a	sgl2c3a3	sgl2c3a1	sgl3c3a2	sgl1-c1a	sgl1-c4a	sgl3c3a2	sgl3c3a1	sgl3c3a3
	Core	Rim	Core	Rim	Core	Core	Rim	Core	Rim	Core
SiO_2	0.07	0.14	0.07	0.15	0.01	0.00	0.00	0.00	0.00	0.00
TiO_2	0.00	0.02	0.00	0.00	0.02	0.00	0.00	0.02	0.03	0.00
Al_2O_3	69.45	68.57	69.32	69.12	70.05	68.95	68.75	69.15	69.01	69.13
Cr_2O_3	0.05	0.09	0.04	0.02	0.00	0.00	0.03	0.02	0.00	0.00
FeO	6.70	6.65	6.86	6.72	7.55	7.55	7.36	7.43	7.28	7.35
MnO	0.11	0.10	0.12	0.12	0.16	0.15	0.16	0.19	0.16	0.15
MgO	23.83	23.63	23.89	23.64	23.09	23.31	23.04	23.42	23.13	23.11
Total	100.21	99.20	100.30	99.77	100.88	99.96	99.34	100.23	99.61	99.74
O	4	4	4	4	4	4	4	4	4	4
Si	0.002	0.003	0.002	0.004	0.000	0.000	0.000	0.000	0.000	0.000
Ti	0.000	0.000	0.000	0.000	0.000	0.000	0.000	0.000	0.000	0.000
Al	1.994	1.989	1.991	1.994	2.005	1.993	1.998	1.993	1.999	2.000
Cr	0.001	0.002	0.001	0.000	0.000	0.000	0.000	0.000	0.000	0.000
Fe	0.136	0.137	0.140	0.138	0.153	0.155	0.152	0.152	0.150	0.151
Mn	0.002	0.002	0.002	0.002	0.003	0.003	0.003	0.004	0.003	0.003
Mg	0.865	0.867	0.867	0.862	0.835	0.852	0.847	0.853	0.847	0.845
Total cation	3.000	3.000	3.003	3.000	2.996	3.003	3.000	3.002	2.999	2.999
Fe^{3+}	0.003	0.005	0.007	0.003	0.000	0.007	0.001	0.006	0.000	0.000
Fe^{2+}	0.133	0.132	0.133	0.135	0.153	0.148	0.150	0.146	0.149	0.151
X_{Mg}	0.864	0.864	0.861	0.862	0.845	0.846	0.848	0.849	0.850	0.848

X_{Mg}=Mg/(Mg+Fe).

Table 3b
Representative spinel trace element analyses

Anal. no.	sgl1
Ti	7.1
V	44.0
Cr	40.5
Co	7.1
Ni	14.7
Cu	0.1
Zn	304.5
Ga	64.0
Ge	3.9
As	3.1
Se	250.5
Sr	0.1
Y	0.1
Zr	0.2
Nb	0.1
Mo	0.4
Pd	0.4
Ag	0.1
Cd	1.0
Sn	0.2
Sb	0.2
I	25.0
Cs	0.2
Ba	0.4
La	0.0
Ce	0.0
Pr	0.0
Nd	0.3
Eu	0.0
Gd	0.3
Tb	0.1
Dy	0.2
Ho	0.3
Er	0.2
Yb	0.2
Lu	0.1
Hf	0.2
Ta	0.1
Th	0.1
U	0.1

Archipelago, Papua New Guinea (Franz and Wirth, 2000) and as inclusions within olivine phenocrysts in primitive arc volcanics (Della-Pasqua et al., 1995). Some models were put forward to explain the genesis of aluminous spinel in ultramafic to mafic rocks, amongst which are: (1) a xenocrystal derivation (e.g. Keuhner et al., 1981; Della-Pasqua et al., 1995), (2) breakdown of pre-existing aluminous minerals such as amphibole or phlogopite (e.g. Wagner and Velde, 1987; Franz and Wirth, 2000), (3) crystallization from a discrete high Al-rich melt in a magma chamber (Jaques and Foley, 1985) and (4) crystallization during unmixing or exsolution of non-stoichiometric leucite in ultrapotassic rocks (Keuhner et al., 1981). These models were capable of explaining the origin of aluminous spinel to some extent, but the processes involved in the formation of a primitive highly aluminous melts within ultramafic–mafic systems still remain mostly ambiguous.

A metamorphic or metasomatic origin for the aluminous spinel by the breakdown of phlogopite by the reaction; Phlogopite→Forsterite+Al-spinel+Melt (Pasteris, 1983) is highly incompatible with the textures observed. Forsterite is not present in this rock. In addition, textures indicative of mineral replacement were not noticed. A xenocrystal origin, i.e., the accidental trapping of aluminous spinel crystals from granulites and gneisses, can also be ruled out, because (1) no fragments of granulite or gneisses were found as enclaves or boudins within the BASP-or adjacent ultramafic rocks and (2) the spinel and mica present in various metamorphic rocks of the study area, and adjacent areas are hercynite and biotite (e.g. Santosh, 1987; Cenki et al., 2002), respectively. No features indicating exsolution to form spinel were observed in studied sections. Therefore, the only plausible model is precipitation of aluminous spinel from localized high Al-melts. The high-Al nature of the rocks is also evident from chemical characteristics of ultramafic rocks present in the eastern and central parts (Rajesh et al., 2004a). The spinel and phlogopite present in all the rock units are highly aluminous. Moreover the dunite possesses ~8 wt.% Al_2O_3 (Rajesh et al., 2004a), which is quite extraordinary in common dunite and other ultramafic rocks. These lines of evidence further substantiate the local super-saturation of parental melt with alumina. The spinel grains are characterized by abundant pure CO_2 fluid inclusions, magnesite and graphite mineral inclusions, and high-temperature melt inclusions (Rajesh, 2004b). This is suggestive of the presence of C—in various forms in the parental melt. The coexistence of CO_2–graphite and graphite–magnesite may indicate the localized variations in oxygen fugacity conditions during their crystallization. The spinel chemistry (Table 3a) confirms their extremely low Fe^{3+} contents suggesting reduced environment of spinel crystallization (Jaques and Foley, 1985; Foley, 1985). Fig. 6 is the compositional variation diagram of spinel from various settings such as mantle restite, arc cumulate and metasomatite in terms of Al_2O_3 and Cr_2O_3 contents (in wt.%) amassed by Franz and Wirth (2000). In this diagram, the spinel from BASP rock plots in a separate non-defined area much above the metasomatic field.

Baddeleyite is one of the rare zirconium-bearing accessory minerals crystallizing during the late stages of the magmatic evolution of alkaline, ultramafic to mafic

Table 4a
Representative major element chemical composition of phlogopites

Anal. no.	sgl1p1	sgl1p2	sgl1p3	sgl1p4	sgl2c7p1	sgl2c7p2	sgl2c7p3	sgl2c7p4	sgl3c1p1	sgl3c1p2	sgl3c1p3	sgl3c1p4
	Rim	Core	Core	Rim	Rim	Core	Core	Rim	Rim	Core	Core	Rim
SiO_2	38.81	38.31	38.17	38.36	38.47	38.44	38.68	38.64	38.50	38.35	38.10	38.09
TiO_2	0.85	0.95	0.97	0.92	0.87	0.90	0.89	0.87	0.85	1.16	1.14	1.08
Al_2O_3	18.09	18.45	18.01	18.11	18.49	18.13	18.35	17.88	19.00	18.91	18.38	18.81
Cr_2O_3	0.00	0.00	0.04	0.00	0.00	0.02	0.00	0.00	0.02	0.04	0.01	0.01
FeO	1.90	1.84	1.94	1.95	1.90	1.89	1.96	1.94	1.95	2.37	2.18	2.30
MnO	0.02	0.00	0.04	0.02	0.04	0.01	0.02	0.00	0.02	0.02	0.02	0.03
MgO	24.14	23.94	23.74	23.82	23.93	24.02	24.00	24.15	24.17	23.32	23.54	23.38
CaO	0.01	0.01	0.02	0.02	0.00	0.00	0.00	0.00	0.03	0.02	0.02	0.06
Na_2O	0.16	0.10	0.13	0.14	0.14	0.13	0.15	0.13	0.15	0.14	0.17	0.18
K_2O	10.51	10.57	10.50	10.53	10.69	10.59	10.75	10.61	10.53	9.66	10.23	10.13
Total	94.49	94.17	93.56	93.87	94.53	94.13	94.80	94.22	95.22	93.99	93.79	94.07
O	22.000	22.000	22.000	22.000	22.000	22.000	22.000	22.000	22.000	22.000	22.000	22.000
Si	5.496	5.446	5.469	5.475	5.454	5.471	5.470	5.494	5.413	5.444	5.442	5.422
Ti	0.091	0.101	0.104	0.099	0.093	0.097	0.095	0.093	0.090	0.123	0.122	0.116
Al	3.020	3.092	3.040	3.046	3.089	3.041	3.057	2.996	3.149	3.163	3.093	3.155
Cr	0.000	0.000	0.004	0.000	0.000	0.002	0.000	0.000	0.003	0.005	0.001	0.001
Fe	0.224	0.219	0.232	0.232	0.225	0.225	0.232	0.231	0.229	0.282	0.261	0.273
Mn	0.002	0.000	0.005	0.002	0.005	0.001	0.002	0.000	0.002	0.002	0.002	0.003
Mg	5.097	5.074	5.070	5.068	5.058	5.095	5.059	5.120	5.066	4.935	5.012	4.961
Ca	0.001	0.001	0.003	0.003	0.000	0.000	0.000	0.000	0.005	0.004	0.003	0.009
Na	0.045	0.028	0.037	0.039	0.038	0.034	0.041	0.035	0.041	0.037	0.048	0.049
K	1.899	1.917	1.919	1.917	1.933	1.923	1.940	1.924	1.888	1.749	1.863	1.839
Total cations	15.875	15.878	15.883	15.881	15.895	15.889	15.896	15.893	15.886	15.744	15.847	15.828
X_{Mg}	0.958	0.959	0.956	0.956	0.957	0.958	0.956	0.957	0.957	0.946	0.951	0.948
X_{Fe}	0.042	0.041	0.044	0.044	0.043	0.042	0.044	0.043	0.043	0.054	0.049	0.052

X_{Mg}=Mg/(Mg+Fe).

magmas (e.g. Lumpkin, 1999). Nevertheless, its occurrence as inclusions within spinel and phlogopite of BASP rock indicates, without doubt, its earlier crystallization from the melt (Rajesh et al., in press). Foley et al. (2002) also proposed the presence of baddeleyite in the parental melts of rift-related carbonate rich ultramafic lamprophyres from the Beaver Lake area of the Eastern Antarctica. The existence of baddeleyite by itself suggests the silica-undersaturated nature of the melts (e.g. Bingen et al., 2001); as with elevated silica activity, most of the baddeleyite (ZrO_2) will react with SiO_2 to form zircon (Lumpkin, 1999; Bingen et al., 2001). We did not identify any zircon/ilmenite/rutile/zirconolite rims, magmatic zoning or metamorphic overgrowth patterns around baddeleyite. Therefore, the possibility of such a transformation is ruled out. All the chemical and petrological characteristics of the minerals clearly indicate the silica-undersaturated nature of the melts responsible for the formation of BASP rock. The chemical characteristic of the baddeleyite observed in this rock is closely comparable with those described from carbonatites. Most of the baddeleyite from carbonatites are characterized by the enrichment of actinide components such as U and Th, and Hf with marked depletion of REEs (Purtscheller and Tessadri, 1985; Zaccarini et al., 2004). For the formation of baddeleyite, a confined over-saturation of Zr is needed, which will take place in a milieu that is favored by high Ca and low Si (Dawson et al., 2001).

Phlogopite is believed to be a vital mineral in the upper mantle that can act as a robust reservoir for alkaline and volatile components, and plays a crucial role in the generation of alkaline magmas (e.g. Arai, 1984, 1986; Beard et al., 1998; Zanetti et al., 1999). The presence of phlogopite itself is revelatory of high-K, Mg and hydrous nature of the melts (Beard et al., 1998). Moreover, Al_2O_3 contents (~18.5 wt.%) of phlogopite also advocate the high-Al nature of the melts responsible for the formation of this peculiar rock. The Mg# of phlogopite is in the range of 95–96, very much similar to that from solid-intrusive peridotite (e.g. Arai and Takahashi, 1989; Zanetti et al., 1999) and kimberlites (e.g. Delaney et al., 1980). Also the K/(K+Na) values (0.97–0.99)

Table 4b
Representative trace element analyses of phlogopite

Anal. no.	sgl1p1	sgl1p2	sgl1p3	sgl1p4	sgl2c7p1	sgl2c7p2	sgl2c7p3	sgl2c7p4	sgl3c1p1	sgl3c1p2	sgl3c1p3	sgl3c1p4
	Rim	Core	Core	Rim	Rim	Core	Core	Rim	Rim	Core	Core	Rim
B	23.5	21.4	18.3	20.7	22.5	22.4	22.4	23.4	22.2	23.8	23.1	20.5
Sc	14.8	14.3	15.0	14.0	15.2	15.6	15.7	15.4	16.2	16.0	16.8	16.6
V	221.6	215.1	220.0	217.9	243.0	244.6	245.6	244.4	243.9	248.5	274.1	247.4
Cr	60.8	59.6	58.6	55.8	32.4	30.1	30.7	31.3	10.7	11.4	10.8	11.7
Mn	158.2	154.2	153.9	151.6	192.4	194.5	196.8	185.7	209.4	197.9	194.1	207.0
Co	3.3	3.2	3.0	3.0	3.2	3.3	3.0	3.1	3.9	3.3	3.2	4.0
Ni	22.7	22.9	23.2	22.0	22.2	23.5	22.9	23.3	23.5	23.3	23.4	24.8
Zn	21.7	21.6	21.1	21.6	23.6	24.4	23.9	25.2	25.3	24.2	27.6	28.7
Ga	53.6	54.7	54.5	53.9	57.9	56.5	58.9	55.4	62.0	61.9	58.3	61.8
Rb	658.9	653.6	665.4	638.0	680.8	677.2	679.9	675.7	666.4	696.1	675.5	672.1
Sr	105.9	88.8	90.7	87.5	49.5	55.7	67.6	48.5	63.6	63.1	61.2	63.6
Y	0.1	0.1	0.1	0.1	0.2	0.3	0.4	4.8	0.2	0.3	0.4	0.7
Zr	27.4	16.1	18.4	17.5	9.1	11.5	13.3	9.7	19.5	17.0	14.6	10.9
Nb	28.1	27.5	27.8	26.9	30.7	30.5	30.7	30.5	30.7	30.9	31.3	31.3
Sn	9.4	9.2	9.1	8.9	9.0	9.0	9.2	9.0	9.0	9.6	8.9	9.2
Cs	60.9	60.8	63.6	60.3	61.1	63.4	62.1	62.6	62.6	63.5	62.9	60.7
Ba	1771.0	1836.9	1874.3	1835.5	1669.4	1601.6	1711.6	1612.9	1614.9	1653.5	1662.8	1704.4
Eu	0.2	0.1	0.1	0.1	0.1	0.1	0.1	0.3	0.1	0.1	0.1	0.1
Hf	1.9	1.4	1.6	1.5	0.7	0.8	1.0	0.8	1.2	1.2	1.0	0.8
Ta	5.2	5.4	5.5	5.1	4.0	3.9	4.0	3.9	4.1	4.1	4.2	4.2
W	2.8	2.1	1.8	2.0	2.0	2.4	2.4	1.5	2.6	2.2	1.3	2.2
Tl	4.7	4.8	4.8	4.4	5.5	5.4	5.5	5.3	5.2	5.6	5.3	5.3
Pb	14.3	12.5	12.8	12.2	13.4	13.7	14.4	13.1	13.1	14.5	12.8	13.9
U	0.2	0.0	0.0	0.0	0.0	bdl	0.0	0.3	0.0	0.0	0.0	0.1

are extremely high, being exactly similar to those from kimberlites (Aoki, 1974; Delaney et al., 1980; Jones et al., 1982; Arai, 1986). These features imply a deep source derivation for phlogopite of BASP rock. Brod et al. (2001) depicted the characteristics of phlogopite in various carbonatites and silica undersaturated rocks of Brazil. In Jacupiranga, they concluded that phlogopite in carbonatites are characterized by high Mg#, very low TiO_2, high MgO, Al_2O_3 and BaO. Krasnova (2001) reported features of low contents of TiO_2 and FeO for phlogopites from Kovdor carbonatites. These geochemical features of phlogopite are described as the differentiation product of a parental carbonatite magma (Gaspar and Wyllie, 1987; Brod et al., 2001). The BASP phlogopite also has high MgO, Al_2O_3 and considerable Ba contents (Tables 4a and b) along with low TiO_2, which is consistent with their derivation from melts having carbonatite affinities. The trace element analysis confirms that the phlogopite in the present rock is an excellent repository for Ba and Rb. Fig. 7 represents the evolution trends of micas in terms of Al, Mg and Fe (p.f.u.) from silica undersaturated rocks, carbonatite and metasomatic rocks compiled by Brod et al. (2001). It is evident from this diagram that compositions of phlogopite in BASP rock plot in the evolutionary trend of carbonatites.

Apatite is one of the main accessory minerals in a wide variety of rock types, especially in mantle-derived silica-undersaturated alkaline rocks. It is the main repository of volatiles such as Cl and F, trace elements like U, Th and Sr and LREEs in the mantle (O'Reilly and Griffin, 2000). The occurrence of apatite probably indicates a derivation from U-enriched mantle regions for the involved magma (O'Reilly and Griffin, 2000). The higher abundance of REEs in apatite than in phlogopite and spinel is indicative of its strong capability to contend with other mineral phases to accommodate significant REEs (e.g. Sha and Chappell, 1999; Belousova et al., 2001, 2002). No other mineral phases are able to accommodate REEs, except baddeleyite in the BASP rock. However, due to its earlier crystallization from the melt, baddeleyite could not accommodate REEs in its crystal structure in the BASP rock. Accordingly, all the REEs in the melt accountable for the formation of this rock favored apatite. Hence, trace element characteristics of apatite will reflect those of the host rocks in the present case (Belousova et al., 2001, 2002; Morishita et al., 2003). The higher total REE concentrations of the apatite are attributable to its derivation from a melt having carbonatite affinities

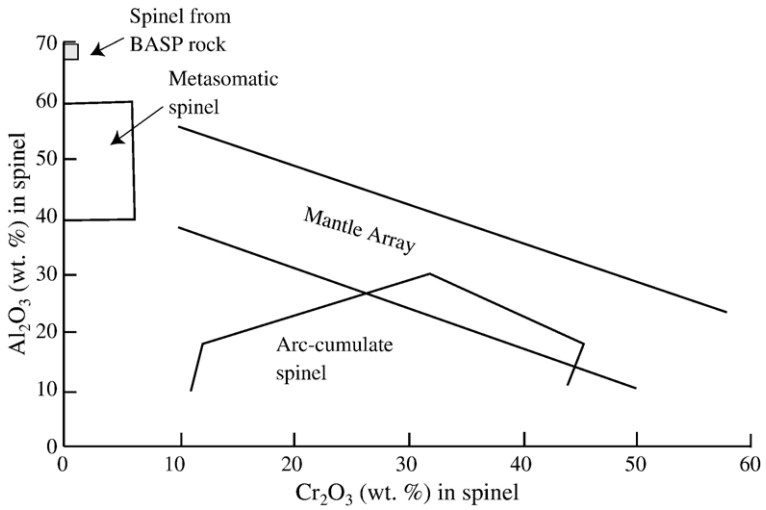

Fig. 6. Al_2O_3 versus Cr_2O_3 (wt.%) diagram for spinel in the BASP rock (after Franz and Wirth, 2000).

(Belousova et al., 2002; Pitawala et al., 2003). The Ce/La ratio of the apatites is ~2; the value is similar to that of most of the apatites found in alkaline igneous and carbonatitic rocks (Fleischer and Altschuler, 1986; Pitawala et al., 2003). In the chondrite normalized diagram (Fig. 5), the apatite shows 10^4 times chondrite values and the negative sloped REE pattern is more or less similar to the carbonatite REE patterns (10^3–10^4 times chondrite; Woolley and Kempe, 1989; Smithies and Marsh, 1998; Bühn et al., 2001). Moreover the observed negative Eu anomaly in apatite is similar to that of the carbonatite-derived melt/fluids (Bühn et al., 1999, 2001). The observed negative Eu anomalies can be accounted by the formation of Eu^{2+} in a reducing environment, i.e., the fractionation of divalent Eu from other trivalent rare earths (Sha and Chappell, 1999; Stalder and Rozendaal, 2004; Takahashi et al., 2005). This environment of formation of apatite may indicate a

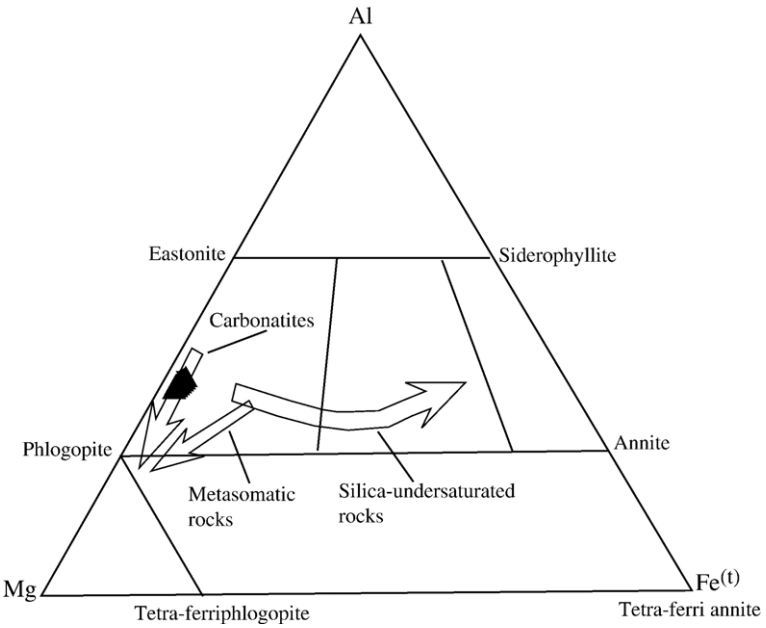

Fig. 7. The composition of phlogopite of present study (solid triangle) in terms of Al, Fe and Mg. The arrows portray evolution trends of micas from silica undersaturated rocks, carbonatites and metasomatic rocks of Jacupiranga carbonatite complex, Brazil. The $Fe^{(t)}$ represents the total iron calculated as Fe^{2+} (modified after Brod et al., 2001).

reduced environment for the formation of BASP rock also. The Th concentration noticed in apatite is more or less similar to those of the whole-rock carbonatites described by several workers (e.g. Woolley and Kempe, 1989; Smithies and Marsh, 1998). The high concentrations of Y and Th would represent the highly evolved residual liquids that remained after the crystallization of carbonatite melts, and are typical of ferrocarbonatites (Smithies and Marsh, 1998). The extreme enrichment of LREEs is typical of apatites in mantle-derived peridotites and carbonatites (Belousova et al., 2002). The bulk rock low concentrations of trace elements such as Ba, Nb, Zr and V are also typical of carbonatites (Woolley and Kempe, 1989). Similar depletions in these incompatible elements can also been observed in the apatites of BASP rock. Even though several dissimilarities are there among the apatites of present and the reported carbonatites, we envisage the crystallization of apatite, and other minerals of BASP rock from a carbonatite-type fluid/melts percolating through the deep-seated shear zone.

The presence of Al-spinel, phlogopite, apatite and baddeleyite in the BASP rock implies that the parental melt was enriched in elements such as Al, Mg, K, Zr, P, Ca, LREEs and actinides like U and Th, trace elements like Ba, Rb, and Sr with abundant volatiles and depleted in Si. The only silicate mineral present in the rock is phlogopite, which itself is a silica-undersaturated mineral. Based on the mineralogy and inclusion studies it can be briefed that the dominant volatiles present in the rock are H_2O, CO_2 and halogens like F and Cl. The whole rock geochemistry of carbonatite rocks might not reflect the original composition of the parental melt, because it may loose highly mobile alkali and volatile components during cooling due to its low viscosity (Bühn et al., 1999). Hence, they recommended a combined study of alkaline fluids/melts/volatiles entrapped as inclusions within the major minerals to reveal the pristine melt compositions. The spinel in the present rock contains abundant high-T melt, pure CO_2-fluid, and magnesite and graphite mineral inclusions as revealed by laser Raman spectra and the microthermometric analysis (Rajesh, 2004b). At present, we do not have the compositional data of the entrapped melts. The baddeleyite is found as inclusions in spinel and phlogopite, and is devoid of any mineral inclusions. This observation probably points towards the coeval nature of the melt entrapment and baddeleyite formation, and implies the localised Zr and actinide enrichment/supersaturation of melts. Hence, it is evident that the parental melts of present rock has carbonatite-favored volatiles (C in both oxidized and reduced form), magnesium carbonate and actinides like U and Th.

6.2. Probable model for the origin of BASP rock

The generation of alkaline magmas/melts including carbonatites is intimately related with the extension resulting from the relaxation of the earlier compressive regime after the termination of subduction in many subduction-related tectonic regimes (Liegeois and Black, 1987). These magmas/melts might have been generated in the upper mantle depths and moved upwards into the lower crustal depths through deep-seated open fractures that are not observable at the surface (cf. Leelanandam, 1993). During their upward motion, due to various physico-chemical properties, they are able to alter the composition and mineralogy of preexisting crustal rocks through metasomatic processes. They can precipitate by themselves alkaline/silica undersaturated rocks upon cooling. In the present scenario, we believe that the ACSZ acted as a deep-seated open fracture, through which the melts having alkaline/carbonatite affinities from upper mantle depths (probably) percolated upward to solidify. Carbonatite melts as a type of metasomatising agents that can alter the upper mantle peridotites have been widely reported from many rift-related environments (e.g. Neumann et al., 2002; Wagner et al., 2003). Furthermore, carbonatite melts have low dihedral wetting angles, low viscosities, high separation velocities and diffusivites (Minarik and Watson, 1995; Karmalkar and Sarma, 2003); hence, they are capable of controlling the trace-element budget in the upper mantle and perform as a tremendous mediator of element transportation within the upper mantle. The high concentration of trace elements and REEs in alkaline rocks is interpreted by Philpots (1990) as the small degrees of partial melting of a relatively undepleted mantle in which garnet is stable in the source region. Gittins (1989) suggested that the behavior of halogens (F and Cl), H_2O, CO_2 and P within a particular magmatic melt controls the depletion or enrichment of alkaline components. Coming to the present scenario, based on the petrography, mineralogy and inclusion assemblage, and geochemical characters of individual minerals we can summarize that melts of carbonatite affinities that were channeled through the deep-rooted shear zone are responsible for the formation of BASP rock and subsequent emplacement of the mass. These melts can be a probable carbonatite-metasomatic candidate. Nevertheless, due to the lack of any metasomatic or metasomatized features in the present

rock or other rock units within the ultramafic complex, we reasonably conclude that the unusual and rare rock type such as BASP rock and the peculiar ultramafic rocks within ACSZ (Rajesh et al., 2004a,b) are a kind of cumulate from the melts with carbonatite affinities, which are capable of carbonatitic mantle metasomatism on peridotite. We infer that the BASP rock was emplaced during Early Ordovician in an extensional tectonic regime along the ACSZ.

7. Conclusions

1. The BASP rock is found as an isolated exposure within the close proximity of western part of the unusual ultramafic complex in ACSZ. The mineralogical species combined with the lack of visible deformation in BASP rock suggests its silica-undersaturated nature and emplacement after dominant Pan-African tectonothermal events, respectively.
2. The mineral assemblage of BASP rock, apatite–phlogopite–baddeleyite, is exactly similar to many reported carbonatites, the presence of aluminous spinel turns the rock into a highly unusual one.
3. The spinel in BASP rock is highly aluminous, with abundant CO_2, graphite and magnesite, baddeleyite and high-T melt inclusions. The inclusions within the spinel imply the carbonatite-favored elements involved in the formation of this peculiar rock.
4. The chemical compositions of phlogopite, baddeleyite and apatite are typical of many carbonatites.
5. The negative Eu/Eu* ratio of apatite combined with negligible Fe^{3+} in spinel is suggestive of the formation of melts in a reduced environment.
6. Based on many lines of evidence we anticipate that the BASP rock forms a probable cumulate from melts of carbonatite affinity that were percolated through the deep-seated ACSZ under an extensional regime.

Acknowledgments

V.J. Rajesh (VJR) acknowledges a doctoral fellowship from the Japanese Ministry of Education, Sports, Culture, Science and Technology, and thanks Drs. Y. Ishida, A. Tamura and Y. Shimizu (Department of Earth Sciences, Kanazawa University) for their warm hospitality and valuable assistance in EPMA and LA-ICP-MS analyses. VJR is thankful to Prof. M. Santosh (Kochi University, Japan) for personal discussions during several stages of this work. Thanks are also due to Prof. C.W. Oh and Dr. S.W. Kim for the research facilities in Chonbuk National University. This work has benefited greatly from the constructive reviews of two anonymous reviewers. We thank these reviewers as well as the editor Prof. Stephen F. Foley, for his excellent editorial comments and supports. This is a contribution to the Grant-in-Aid for Scientific Research provided by the Japanese Society for the Promotion of Science (13373005) to Prof. M. Arima (Yokohama National University, Japan), Grant-in-Aid from the Japanese Ministry of Education, Sports, Culture, Science and Technology to Santosh (No. 17403013) and a grant to VJR from the post doctoral program of Chonbuk National University (2004), South Korea. This work is also a contribution to IGCP 368, 440 and 453.

References

Aoki, K., 1974. Phlogopites and potassic richterites from mica nodules in South African Kimberlites. Contributions to Mineralogy and Petrology 48, 1–7.

Arai, S., 1984. Pressure–temperature dependant compositional variation of phlogopitic micas in upper mantle peridotites. Contributions to Mineralogy and Petrology 87, 260–264.

Arai, S., 1986. K/Na variation in phlogopite and amphibole of upper mantle peridotites due to fractionation of the metasomatizing fluids. Journal of Geology 94, 436–444.

Arai, S., 1992. Chemistry of chromian spinel in volcanic rocks as a potential guide to magma chemistry. Mineralogical Magazine 56, 173–184.

Arai, S., 1994a. Characterization of spinel peridotites by olivine–spinel compositional relationships: review and interpretation. Chemical Geology 113, 191–204.

Arai, S., 1994b. Compositional variation of olivine–chromian spinel in Mg-rich magmas as a guide to their residual spinel peridotites. Journal of Volcanology and Geothermal Research 59, 279–293.

Arai, S., Takahashi, N., 1989. Formation and compositional variation of phlogopites in the Horoman peridotite complex, Hokkaido, northern Japan: implications for origin and fractination of metasomatic fluids in the upper mantle. Contributions to Mineralogy and Petrology 101, 165–175.

Bartlett, J.M., Dougherty-Page, J.S., Harris, N.B.W., Hawkesworth, C.J., Santosh, M., 1998. The application of single zircon evaporation and model Nd ages to the interpretation of polymetamorphic terrains: an example from the Proterozoic mobile belt of south India. Contributions to Mineralogy and Petrology 131, 181–195.

Beard, A.D., Downes, H., Hegner, E., Sablukov, S.M., Vetrin, V.R., Balogh, K., 1998. Mineralogy and geochemistry of Devonian ultramafic minor intrusions of the southern Kola Peninsula, Russia: implications for the petrogenesis of kimberlites and melilites. Contributions to Mineralogy and Petrology 130, 288–303.

Belousova, E.A., Walters, S., Griffin, W.L., O'Reilly, S.Y., 2001. Trace element signatures of apatites from granitoids of Mount Isa Inlier, north-west Queensland, Australia. Australian Journal of Earth Sciences 48, 603–619.

Belousova, E.A., Griffin, W.L., O'Reilly, S.Y., Fisher, N.I., 2002. Apatite as an indicator mineral for mineral exploration: trace-element compositions and their relationship to host rock type. Journal of Geochemical Exploration 76, 45–69.

Bingen, B., Austrheim, H., Whitehouse, M., 2001. Ilmenite as a source for zirconium during high-grade metamorphism? Textural evidence from the Caledonides of Western Norway and implications for zircon geochronology. Journal of Petrology 42, 355–375.

Brandon, A.D., Meen, J.K., 1995. Nd isotopic evidence for the position of southernmost Indian terranes within East Gondwana. Precambrian Research 70, 269–280.

Braun, I., Kriegsman, L.M., 2003. Proterozoic crustal evolution of southernmost India and Sri Lanka. In: Yoshida, M., Windley, B.F., Dasgupta, S. (Eds.), Proterozoic East Gondwana: Supercontinent Assembly and Breakup, vol. 206. Geological Society of London Special Publication, pp. 169–202.

Braun, I., Montel, J.-M., Nicollet, C., 1998. Electron microprobe dating of monazites from high-grade gneisses and pegmatites of the Kerala Khondalite Belt, southern India. Chemical Geology 146, 65–85.

Brod, J.A., Gaspar, J.C., de Araújo, D.P., Gibson, S.A., Thompson, R.N., Junqueira-Brod, T.C., 2001. Phlogopite and tetra-ferriphlogopite from Brazilian carbonatite complexes: petrogenetic constraints and implications for mineral-chemistry systematics. Journal of Asian Earth Sciences 19, 265–296.

Bühn, B., Rankin, A.H., Radtke, M., Haller, M., Knöchel, A., 1999. Burbankite, a (Sr,REE,Na,Ca)-carbonate in fluid inclusions from carbonatite-derived fluids: identification and characterization using Laser Raman spectroscopy, SEM-EDX, and synchrotron micro-XRF analysis. American Mineralogist 84, 1117–1125.

Bühn, B., Wall, F., Le Bas, M.J., 2001. Rare-earth element systematics of carbonatitic flourapatites, and their significance for carbonatite magma evolution. Contributions to Mineralogy and Petrology 141, 572–591.

Cartwright, I., Buick, I.S., Foster, D.A., Lambert, D.D., 1999. Alice Springs age shear zones from the Reynolds Range, central Australia: implications for regional tectonics. Australian Journal of Earth Sciences 46, 355–363.

Cenki, B., Kriegsman, L., Braun, I., 2002. Melt producing and melt-consuming reactions in the Achankovil cordierite gneiss, South India. Journal of Metamorphic Geology 20, 543–561.

Cenki, B., Braun, I., Bröcker, M., 2004. Evolution of the continental crust in the Kerala Khondalite Belt, southernmost India: evidence from Nd isotope mapping combined with U–Pb and Rb–Sr geochronology. Precambrian Research 134, 275–292.

Dawson, J.B., Hill, P.G., Kinny, P.D., 2001. Mineral chemistry of a zircon, composite, veined and metasomatised upper-mantle peridotite xenolith from kimberlite. Contributions to Mineralogy and Petrology 140, 720–733.

Delaney, J.S., Smith, J.V., Carswell, D.A., Dawson, J.B., 1980. Chemistry of micas from kimberlites and xenoliths: II. Primary- and secondary-textured micas from peridotite xenoliths. Geochimica et Cosmochimica Acta 44, 857–872.

Della-Pasqua, F.N., Kamenetsky, V.S., Gasparon, M., Crawford, A.J., Varne, R., 1995. Al-spinels in primitive arc volcanics. Mineralogy and Petrology 53, 1–26.

Dick, H.J.B., Bullen, T., 1984. Chromian spinel as a petrogenetic indicator in abyssal and alpine-type peridotites and spatially associated lavas. Contributions to Mineralogy and Petrology 86, 54–76.

Drury, S.A., Holt, R.W., 1980. The tectonic framework of the South Indian craton: a reconnaissance involving LANDSAT imagery. Tectonophysics 65, T1–T5.

Drury, S.A., Harris, N.B.W., Holt, B.W., Reeves-Smith, G.J., Wightman, R.T., 1984. Precambrian tectonics of crustal evolution in South India. Journal of Geology 92, 3–20.

Fleischer, M., Altschuler, Z.S., 1986. The lanthanides and yttrium in minerals of the apatite group—an analysis of the available data. Neues Jahrbuch für Mineralogie Monatshefte 10, 467–480.

Foley, S.F., 1985. The oxidation state of the lamproitic magmas. Tschermaks Mineralogische und Petrographische Mitteilungen 34, 217–238.

Foley, S.F., Andronikov, A.V., Melzer, S., 2002. Petrology of ultramafic lamprophyres from the Beaver Lake area of eastern Antarctica and their relation to the breakup of Gondwanaland. Mineralogy and Petrology 74, 361–384.

Franz, L., Wirth, R., 2000. Spinel inclusions in olivine of peridotite xenoliths from TUBAF seamount (Bismark Archipelago/Papua New Guinea): evidence for the thermal and tectonic evolution of the oceanic lithosphere. Contributions to Mineralogy and Petrology 140, 283–295.

Gaspar, J.C., Wyllie, P., 1987. The phlogopites from the Jacupiranga carbonatite intrusions. Mineralogy and Petrology 36, 121–134.

Gittins, J., 1989. The origin and evolution of carbonatite magmas. In: Bell, K. (Ed.), Carbonatites: Genesis and Evolution. Unwin Hyman, London, UK, pp. 580–600.

Harris, N.B.W., Santosh, M., Taylor, P.N., 1994. Crustal evolution in South India: constraints from Nd isotopes. Journal of Geology 102, 139–150.

Heaman, L.M., Le Cheminant, A.N., 1993. Paragenesis and U–Pb systematics of baddeleyite (ZrO_2). Chemical Geology 110, 95–126.

Irving, A.J., 1978. A review of experimental studies of crystal/liquid trace element partitioning. Geochimica et Cosmochimica Acta 42, 743–770.

Ishida, Y., Morishita, T., Arai, S., Shirasaka, M., 2004. Simultaneous in-situ multi-element analysis of minerals on thin section using LA-ICP-MS. The Science Reports of Kanazawa University 48, 31–42.

Jaques, A.L., Foley, S.F., 1985. The origin of Al-rich spinel inclusions in leucite from the leucite lamproites of Western Australia. American Mineralogist 70, 1143–1150.

Jones, A.P., Smith, J.V., Dawson, J.B., 1982. Mantle metasomatism in 14 veined peridotites for Bulfontein mine, South Africa. Journal of Geology 90, 435–453.

Karmalkar, N.R., Sarma, K.P., 2003. Characterization and origin of silicic and alkali-rich glasses in the upper mantle-derived spinel peridotite xenoliths from alkali basalts, Deccan Trap, Kutch, northwest India. Current Science 85, 386–392.

Keuhner, S.M., Edgar, A.D., Arima, M., 1981. Petrogenesis of the ultrpaotassic rocks from the Leucite Hills, Wyoming. American Mineralogist 66, 663–677.

Krasnova, N.I., 2001. The Kovdor phlogopite deposit, Kola Peninsula, Russia. Canadian Mineralogist 39, 33–44.

Kröner, A., Brown, L., 2005. Structure, composition and evolution of the South Indian and Sri Lankan granulite terrains from deep seismic profiling and other geophysical and geological investigations: a LEGENDS initiative. Gondwana Research 8, 317–335.

Leelanandam, C., 1993. Alkaline magmatism in the Eastern Ghat Belt—a critique. Journal of Geological Society of India 42, 435–447.

Liegeois, J.P., Black, R., 1987. Alkaline magmatism subsequent to collision in the Pan-African belt of the Adrar des Iforas (Mali). In: Fitton, J.G., Upton, B.G.J. (Eds.), Alakline Igneous Rocks, vol. 30. Geological Society Special Publication, pp. 381–401.

Longerich, H., Jackson, S.E., Günther, E., 1996. Laser ablation inductively coupled plasma mass spectrometric transient signal

data acquisition and analyte concentration calculation. Journal of Analytical Atomic Spectrometry 11, 899–904.

Lumpkin, G.R., 1999. Physical and chemical characteristics of baddeleyite (monoclinic zirconia) in natural environments: an overview and case study. Journal of Nuclear Materials 274, 206–217.

McCaig, A.M., 1997. The geochemistry of volatile fluid flow in shear zones. In: Holness, M.B. (Ed.), Deformation-Enhanced Fluid Transport in the Earth's Crust and Mantle. Chapman Hall, London, pp. 227–266.

Mikuchi, E.J., Ridley, J.R., 1993. The hydrothermal fluid of Archaean lode gold deposits at different metamorphic grades: compositional constraints from ore and wall rock alteration assemblages. Mineralium Deposita 28, 469–481.

Minarik, W.G., Watson, E.B., 1995. Interconnectivity of carbonate melt at low melt fraction. Earth and Planetary Science Letters 133, 423–437.

Morishita, T., Arai, S., Tamura, A., 2003. Petrology of an apatite-rich layer in the Finero phlogopite-peridotite, Italian Western Alps; implications for evolution of a metasomatising agent. Lithos 69, 37–49.

Morishita, T., Ishida, Y., Arai, S., 2005. Simultaneous determination of multiple trace element compositions in thin (<30 *f*Êm) layers of BCR-2G by 193 nm ArF excimer laser ablation-ICP-MS: implications for matrix effect and element fractionation on quantitative analysis. Geochemical Journal 39, 327–340.

Nandakumar, V., Harley, S.L., 2000. A reappraisal of the pressure temperature path of granulites from the Kerala Khondalite Belt, southern India. Journal of Geology 108, 687–703.

Neumann, E.-R., Wulff-Pedersen, E., Pearson, N.J., Spenger, E.A., 2002. Mantle xenoliths from Tenerife (Canary Islands): evidence for reactions between mantle peridotites and silicic carbonatite melts inducing Ca metasomatism. Journal of Petrology 43, 825–857.

O'Reilly, S., Griffin, W.L., 2000. Apatite in the mantle: implications for metasomatic processes and high heat production in Phanerozoic mantle. Lithos 53, 217–232.

Pasteris, J.D., 1983. Spinel zonation in the De Beers kimberlite, South Africa: possible role of phlogopite. Canadian Mineralogist 21, 41–58.

Pearce, N.J.G., Perkins, W.T., Westgate, J.A., Gorton, M.P., Jackson, S.E., Neal, C.R., Chenery, S.P., 1997. A compilation of new and published major and trace element data for NIST SRM 610 and NIST SRM 612 glass reference materials. Geostandards Newsletter 21, 115–144.

Philpots, A.R., 1990. Principles of Igneous and Metamorphic Petrology. Prentice-Hall, Inc., Englewood Cliffs, U.S.A., 498 pp.

Pitawala, A., Schidlowski, M., Dahanayake, K., Hofmeister, W., 2003. Geochemical and petrological characteristics of Eppawala phosphate deposits, Sri Lanka. Mineralium Deposita 38, 505–515.

Purtscheller, F., Tessadri, R., 1985. Zirconolite and baddeleyite from metacarbonates of the Oetztal-Stubai complex (northern Tyrol, Austria). Mineralogical Magazine 49, 523–529.

Rajaram, M., Harikumar, P., Brown, M., 2003. Thin magnetic crust in the Southern Granulite Terrane. In: Ramakrishnan, M. (Ed.), Tectonics of Southern Granulite Terrane, vol. 50. Geological Society of India Memoir, pp. 165–176.

Rajesh, H.M., 2004a. The igneous charnockites–high-K alkali-calcic I-type granite–incipient charnockite association in Trivandrum Block, southern India. Contributions to Mineralogy and Petrology 147, 346–362.

Rajesh, V.J., 2004b. Graphite–dolomite–phlogopite bearing ultramafic rocks in Achankovil Shear Zone, South India: implications for highly potassic carbon-rich fluid influx along an intracontinental shear zone. Ph.D. thesis, Yokohama National University, Japan.

Rajesh, H.M., Santosh, M., Yoshida, M., 1996. The felsic magmatic province in East Gondwana: implications for Pan-African tectonics. Journal of Southeast Asian Earth Sciences 14, 275–291.

Rajesh, V.J., Arima, M., Santosh, M., 2004a. Dunite, glimmerite and spinellite in Achankovil Shear Zone, South India: highly potassic CO_2-rich melt influx along an intra-continental shear zone. Gondwana Research 7, 961–974.

Rajesh, V.J., Arima, M., Santosh, M., 2004b. First report on zirconolite and baddeleyite from Achankovil Shear Zone, South India. Gondwana Research 7, 1370–1373.

Rajesh, V.J., Yokoyama, K., Santosh, M., Arai, S., Oh, C.W., Kim, S. W., (in press). Zirconolite and baddeleyite in an ultramafic suite from southern India: early Ordovician carbonatite-type melts associated with extensional collapse of the Gondwana crust. Journal of Geology 114.

Sack, R.O., Ghiorso, M.S., 1991. Chromian spinels as petrogenetic indicators: thermodynamics and petrological applications. American Mineralogist 76, 827–847.

Santosh, M., 1987. Cordierite gneisses of South Kerala, India: petrology, fluid inclusions and implications on uptlift history. Contributions to Mineralogy and Petrology 97, 343–356.

Santosh, M., 1996. The Trivandrum and Nagercoil granulite blocks. In: Santosh, M., Yoshida, M. (Eds.), The Archean and Proterozoic Terrains of Southern India Within East Gondwana. Gondwana Research. Group Memoir, vol. 3, pp. 243–277.

Santosh, M., Yokoyama, K., Biju-Sekhar, S., Rogers, J.J.W., 2003. Multiple tectonothermal events in the granulite blocks of southern India revealed from EPMA dating: implications on the history of supercontinents. Gondwana Research 6, 29–63.

Santosh, M., Tanaka, K., Yokoyama, Y., Collins, A.S., 2005. Late Neoproterozoic–Cambrian felsic magmatism along transcrustal shear zones in southern India: U–Pb electron microprobe ages and implications for the amalgamation of the Gondwana supercontinent. Gondwana Research 8, 31–42.

Schulze, D.J., 2001. Origins of chromian and aluminous spinel macrocrysts from kimberlites in southern Africa. Canadian Mineralogist 39, 361–376.

Seifert, W., Kämpf, H., Wasternack, J., 2000. Compositional variation in apatite, phlogopite and other accessory minerals of the ultramafic Delitzsch complex, Germany: implication for cooling history of carbonatites. Lithos 53, 81–100.

Sha, L.-K., Chappell, B.W., 1999. Apatite chemical composition, determined by electron microprobe and laser-ablation inductively coupled plasma mass spectrometry, as a probe into granite petrogenesis. Geochimica et Cosmochimica Acta 63, 3861–3881.

Smithies, R.H., Marsh, J.S., 1998. The Marinks Quellen carbonatite complex, southern Namibia; carbonatite magmatism with an uncontaminated depleted mantle signature in a continental setting. Chemical Geology 148, 201–212.

Stalder, M., Rozendaal, A., 2004. Apatite nodules as an indicator of depositional environment and ore genesis for the Mesoproterozoic Broken Hill-type Gamsberg Zn–Pb deposit, Namaqua Province, South Africa. Mineralium Deposita 39, 189–203.

Sun, S.S., McDonough, W.F., 1989. Chemical and isotopic systematics of oceanic basalts: implications for mantle compositions and

processes. In: Saunders, A.D., Norry, M.J. (Eds.), Magmatism in the Ocean Basins, vol. 42. Geological Society of London, Special Publication, pp. 313–345.

Takahashi, Y., Kolonin, G.R., Shironosova, G.P., Kupriyanova, I.I., Uruga, T., Shimizu, H., 2005. Determination of the Eu(||)/Eu(|||) ratios in minerals by X-ray absorption near-edge structure (XANES) and its application to hydrothermal deposits. Mineralogical Magazine 69, 179–190.

Treloar, P.J., Colley, H., 1996. Variation in F and Cl contents in apatites from magnetite–apatite ores in northern Chile, and their ore-genetic implications. Mineralogical Magazine 60, 285–301.

Venturelli, G., Capedri, S., di Battistini, G., Crawford, A., Kogarko, L. N., Celestini, S., 1984. The ultrapotassic rocks from southeastern Spain. Lithos 17, 37–54.

Wagner, C., Velde, D., 1987. Aluminous spinel in lamproites: occurrence and probable significance. American Mineralogist 72, 689–696.

Wagner, C., Mokhtari, A., Deloule, E., Chabaux, F., 2003. Carbonatite and alkaline magmatism in Taourirt (Morocco): petrological, geochemical and Sr–Nd isotope characteristics. Journal of Petrology 44, 937–965.

Windley, B.F., Razafiniparany, A., Razakamana, T., Ackermand, D., 1994. Tectonic framework of the Precambrian of Madagascar and its Gondwana connections: a review and reappraisal. Geologische Rundschau 83, 642–659.

Woolley, A.R., Kempe, D.R.C., 1989. Carbonatites: nomenclature, average chemical compositions, and element distribution. In: Bell, K. (Ed.), Carbonatites: Genesis and Evolution. Unwin Hyman, London, UK, pp. 1–14.

Zaccarini, F., Stumpfl, E.F., Garuti, G., 2004. Zirconolite and Zr–Th–U minerals in chromitites of the Finero complex, Western Alps, Italy: evidence for carbonatite-type metasomatism in a subcontinental mantle plume. Canadian Mineralogist 42, 1825–1845.

Zanetti, A., Mazzucchelli, M., Rivalenti, G., Vannucci, R., 1999. The Finero phlogopite-peridotite massif: an example of subduction-related metasomatism. Contributions to Mineralogy and Petrology 134, 107–122.